Hindawi Publishing Corporation
Advances in Optical Technologies
Volume 2008, Article ID 615393, 11 pages
doi:10.1155/2008/615393

Research Article

Quantum Electrodynamic Modeling of Silicon-Based Active Devices

Shouyuan Shi, Brandon Redding, Tim Creazzo, Elton Marchena, and Dennis W. Prather

Department of Electrical and Computer Engineering, University of Delaware, Newark, DE 19716, USA

Correspondence should be addressed to Shouyuan Shi, sshi@ee.udel.edu

Received 25 February 2008; Accepted 2 May 2008

Recommended by Pavel Cheben

We propose a time-domain analysis of an active medium based on a coupled quantum mechanical and electromagnetic model to accurately simulate the dynamics of silicon-based photonic devices. To fully account for the nonlinearity of an active medium, the rate equations of a four-level atomic system are introduced into the electromagnetic polarization vector. With these auxiliary differential equations, we solve the time evolution of the electromagnetic waves and atomic population densities using the FDTD method. The developed simulation approach has been used to model light amplification and amplified spontaneous emission in silicon nanocrystals, as well as the lasing dynamics in a novel photonic crystal-based silicon microcavity.

1. INTRODUCTION

Silicon, owing to its excellent electronic material properties, availability, and efficient processing, has played major roles in microelectronics during past decades and promises to be the key material in the foreseeable future. However, the rapid progress of microprocessors will soon be limited by the transmission bandwidth capability of electronic connections. To eliminate the bottleneck of electronic circuits and establish interconnection links between circuit boards, between chips on a board, or even with a single chip, research into silicon microphotonics, which merges the power of silicon microeletronics with the advantages of photonics, has attracted increasing attention in recent years [1, 2].

While a wide variety of passive silicon photonic devices have been developed, recent activities have focused on achieving active functionalities, particularly light amplification and generation, in silicon photonic devices [3–5]. However, due to the fundamental limitation related to the indirect nature of the bulk Si band gap, this semiconductor has very low-light emission efficiency. As a result, the development of silicon light emitters, amplifiers, and lasers has become one of the central goals in the advancement of silicon photonics and optoelectronics. Another driving force stimulating research is the need for low-cost photonic devices for applications related to future computing and communication systems. In the past, a number of different approaches have been taken to overcome silicon's fundamental limitations including silicon nanocrystals, Er-doped Si–Ge, Si–Ge quantum dots, and Er-doped silicon nanocrystals [6–10]. More recently, stimulated Raman scattering has been used to demonstrate light amplification and lasing in silicon, both in pulse and continuous-wave operation [11, 12].

As a result, there is a need for optimal design solutions and physical insight in the field of quantum optics, encompassing applications such as laser systems, amplifiers, laser cooling of atoms, quantum computing, plasmons, polaritons, and enhanced spontaneous emission in microcavities. To address this, various approaches based on quantum electrodynamics, in which the atoms in active systems are treated quantum mechanically but the electromagnetic wave is treated classically, have been developed. In this way, light interaction with an active medium can be studied using a classical harmonic oscillator model and the rate equations of electron population density. Although, simple analytic expressions can be derived for well-defined problems, precise solutions for a realistic system require a numerical solution, particularly in nanophotonic devices.

In addition, over the past several years, numerous methods have been proposed to account for material dispersion, absorption, and gain using the finite-difference and time-domain (FDTD) method [13–17]. One of the most

commonly used and the memory-efficient algorithms is the auxiliary differential equation (ADE) FDTD scheme which accounts for the rate equations that determine the electron energy states' population densities during the propagation of pump and input signals. The approach has been widely used to characterize the absorption in a two-level atomic system [13], gain in a four-level atomic system [14–16, 18], and more complicated lasing dynamics in a four-level two-electron atomic system [19].

In this paper, we present a time-domain analysis of amplification, amplified spontaneous emission (ASE), and lasing dynamics in silicon-based nanophotonic devices based on a coupled quantum mechanical and electromagnetic model. In order to simulate quantum electrodynamics, we incorporate the rate equations of a four-level atomic system to characterize the gain and absorption of an active material. Both amplification and ASE with the assistance of a microcavity are investigated in one-dimensional (1D) and two-dimensional (2D) silicon nanocrystals (Si-ncs). To study lasing dynamics, a novel silicon microcavity based on the unique dispersion properties of photonic crystals is introduced.

2. COUPLED RATE EQUATIONS AND ELECTROMAGNETIC DYNAMICS MODEL

To achieve light amplification and lasing behavior in silicon photonic devices, the development of gain media is essential for the successful design of next generation integrated photonics [4, 5]. As many material systems, such as nanocrystals and Er-doped glasses, have been extensively explored and found to not only experimentally demonstrate photoluminescence for the application of a silicon-based emitter, but also exhibit net gain for the development of a silicon based laser [3, 6–8, 20, 21]. Due to strong coupling between the quantum state and nanoscale electromagnetic waves, a mathematical model is necessary to intimately link quantum mechanical effects to the electromagnetic interaction. To this end, we take both field evolution and material dynamics, such as the dispersive and nonlinear properties, into modeling consideration.

The classical electron oscillator (CEO) model has been widely used to bridge the link between the quantum world and electromagnetic waves. Such quantum-based dynamics are dictated by rate equations which simulate the time evolution of atomic-energy-level populations in the gain medium. The electromagnetic dynamics are dictated by the electromagnetic wave equations [22]. The CEO model allows us to couple these domains and study devices in which the material properties affect the electromagnetic field and vice versa. Depending on the material system, various distinguished energy levels are used to represent its quantum processes, stimulated, and spontaneous emission. As an example, Er-doped glass has been applied as an application of optical amplifier in the field of fiber optics, that is, Er-doped fiber amplifier (EDFA) [18, 23]. A simple four-level model of rate equations is employed to successfully characterize the light amplification. In the presented work, we will apply a similar model for the design of a silicon photonic microcavity.

Recently, the direct observation of photoluminescence (PL) reveals the potential for optical gain in Si-ncs. Although a full theoretical model for the stimulated emission is still not enough, conventional rate equations can be employed to describe the active and nonlinear properties of Si-ncs [9, 10, 24]. Under the first order of approximation, the Auger process is neglected to phenomenologically study the gain medium. A more general model interested in analyzing gain saturation and other higher-order effects could incorporate additional transitions into the rate equation model to represent Auger-type processes, as discussed in [21]. As a consequence, we can further simplify the rate equations to a four-level atomic system. Coupled with Maxwell's equations, we are able to model the time evolution of the atomic-energy-level population density as well as the optical signal propagation, amplification, and absorption in candidate devices.

As shown in Figure 1, time-domain population dynamics can be expressed with a four-level rate equation formulism:

$$\begin{aligned}
\frac{dN_3(t)}{dt} &= -\frac{N_3(t)}{\tau_{32}} + W_p N_0,\\
\frac{dN_2(t)}{dt} &= \frac{N_3(t)}{\tau_{32}} - \frac{N_2(t)}{\tau_{21}} + \frac{1}{\hbar\omega_s}\mathbf{E}(t)\cdot\frac{d\mathbf{P}(t)}{dt},\\
\frac{dN_1(t)}{dt} &= \frac{N_2(t)}{\tau_{21}} - \frac{N_1(t)}{\tau_{10}} - \frac{1}{\hbar\omega_s}\mathbf{E}(t)\cdot\frac{d\mathbf{P}(t)}{dt},\\
\frac{dN_0(t)}{dt} &= \frac{N_1(t)}{\tau_{10}} - W_p N_0,
\end{aligned} \tag{1}$$

where $N_i\,(i = 0,1,2,3)$ are the transition population densities for different atomic levels, which are related to the total concentration $N_{\text{tot}} = \sum_{i=0}^{3} N_i$. τ_{ij} are the lifetimes associated with the transitions from energy E_i to E_j. ω_s is the central frequency of radiation of the materials related to the atomic transition energy levels through $\omega_s = (E_2 - E_1)/\hbar$ and $(1/\hbar\omega_s)\mathbf{E}(t)\cdot d\mathbf{P}(t)/dt$ is the induced radiation rate or excitation rate depending on its sign. The pump rate W_p is defined as $W_p = \sigma_p I_p/\hbar\omega_p$, where σ_p is the absorption cross section, $I_p/\hbar\omega_p$ is the photon flux, and I_p is the intensity of the pumping signal.

Based on the CEO model, the net macroscopic polarization $\mathbf{P}(t)$ induced in the presence of an applied electric field $\mathbf{E}(t)$ for an isotropic medium can be described by the following equations [22]:

$$\frac{d^2\mathbf{P}(t)}{dt^2} + \Delta\omega_s\frac{d\mathbf{P}(t)}{dt} + \omega_s^2\mathbf{P}(t) = \kappa\Delta N_{12}(t)\mathbf{E}(t), \tag{2}$$

where $\Delta N_{12}(t)$ is the instantaneous population density difference between energy levels 1 and 2 of an atomic transition, given by $\Delta N_{12}(t) = N_1(t) - N_2(t)$. The coupling coefficient, κ, determines the strength of the interaction between the quantum and electromagnetic world. It can be easily derived from the above equation that the amplification line shape is Lorentzian and homogeneously broadened, and can be considered as a quantum mechanically correct equation for the induced polarization density in a real

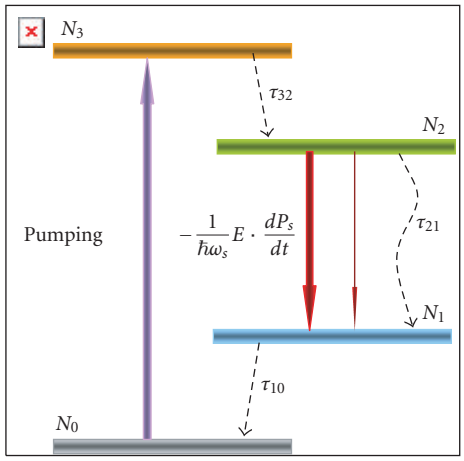

Figure 1: An effective four-atomic-level system to qualitatively model the recombination dynamics under the gain condition.

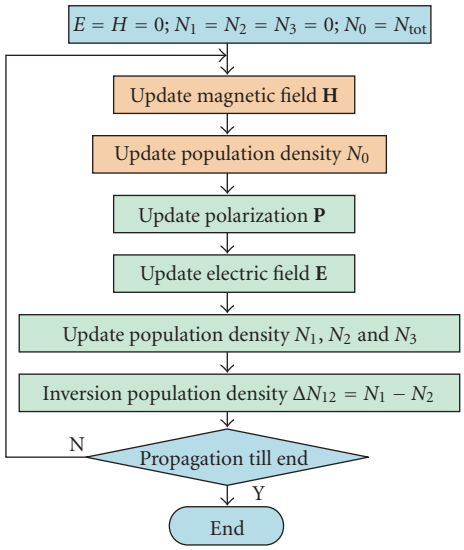

Figure 2: Flow chart of time evolution of population density functions and electromagnetic waves.

atomic system. To excite the system, an optical pumping source that is homogeneously distributed across the device is introduced into the system. Amplification takes place when the external pumping mechanism produces a population inversion $\Delta N_{12}(t) < 0$.

In addition, in the frequency domain, the polarization due to the gain or absorption materials can be derived from (2) as

$$[(\omega^2 - \omega_s^2) + j\omega\Delta\omega_s]\mathbf{P} = \kappa\Delta N_{12}\mathbf{E}. \tag{3}$$

The material susceptibility can then be introduced as $\mathbf{P} = \varepsilon_0\chi\mathbf{E}$. Assuming the host material has a relative dielectric constant of ε_r, the complex dielectric constant can be expressed as

$$\varepsilon_s = \varepsilon_0(\varepsilon_r + \chi_s) = \varepsilon_0\left(\varepsilon_r + \frac{\kappa\Delta N_{12}/\varepsilon_0}{[(\omega^2 - \omega_s^2) + j\omega\Delta\omega_s]}\right). \tag{4}$$

If a plane wave is propagating in such a material, then the imaginary part of the wave vector can be considered as the amplification or absorption coefficient, given by

$$\alpha_s(\omega) = \frac{\pi}{\lambda}\sqrt{\varepsilon_r}\,\mathrm{Im}(\chi_s). \tag{5}$$

On the other hand, if we know the radiative cross-section, σ_s, of the gain medium at peak gain frequency ω_s, the amplification coefficient can be written as

$$\alpha_s = -\frac{\sigma_s\Delta N_{12}}{2}. \tag{6}$$

As a result, we can relate the coupling coefficient with the radiative cross-section through the amplification coefficient as

$$\kappa = c\varepsilon_0\sqrt{\varepsilon_r}\sigma_s\Delta\omega_s. \tag{7}$$

In this manner, we can obtain a coupling coefficient based on experimental observations.

3. AUXILIARY DIFFERENTIAL EQUATIONS FDTD ANALYSIS

With coupled rate and Maxwell's equations, we introduce FDTD to numerically simulate amplification and lasing dynamics. The central difference method can be applied to discretize the electromagnetic field components, the atomic populations of different levels, and the induced polarizations in space and time. Then time marching of electromagnetic waves in leapfrog fashion can be constructed, and consequently the atomic evolutions can be monitored. The electromagnetic waves are governed by Maxwell's equation as

$$\nabla\times\mathbf{E} = -\mu_0\frac{\partial\mathbf{H}}{\partial t}, \qquad \nabla\times\mathbf{H} = \varepsilon_0\varepsilon_r\frac{\partial\mathbf{E}}{\partial t} + \frac{\partial\mathbf{P}}{\partial t} + \mathbf{J}. \tag{8}$$

We briefly describe the discretization algorithm as shown in Figure 2, at time $(n + 0.5)\Delta t$, we first update the magnetic field components and population density N_0. Then, we update the induced polarization based on (2) at time $(n + 1)\Delta t$, where the knowledge of two preceding steps is required. With the known magnetic field and induced polarization, we can calculate the electric field components. At time $(n+1)\Delta t$, we also update the remaining atomic population densities: N_3, N_2, and N_1. Since the population density at the highest energy level, N_3, is related only to N_0 which was updated at the half-time step, the population density is computed in order from high to low levels to maintain consistency and minimize the memory storage.

To excite the system, a source, **J**, must be introduced. Two different sources are considered, one to investigate spontaneous emission and one to investigate stimulated emission. To characterize the amplification (stimulated emission) of an active medium, we launch a probe signal into the system. With the presence of a pumping signal, population inversion takes place within the active medium. As a result, the probe signal is amplified during propagation through the medium.

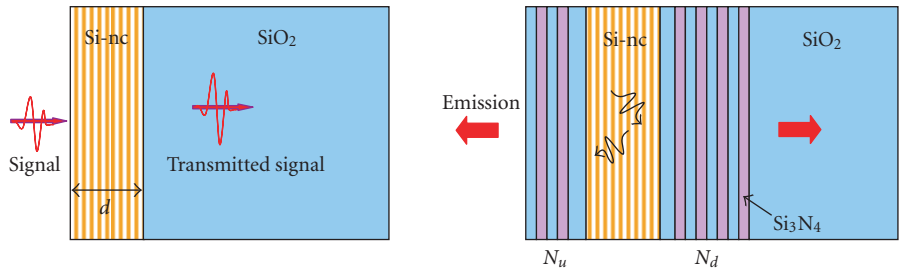

FIGURE 3: (a) 1D Si-nc active device for stimulated emission simulation study. (b) 1D Si-nc active device for amplified stimulated emission simulation study.

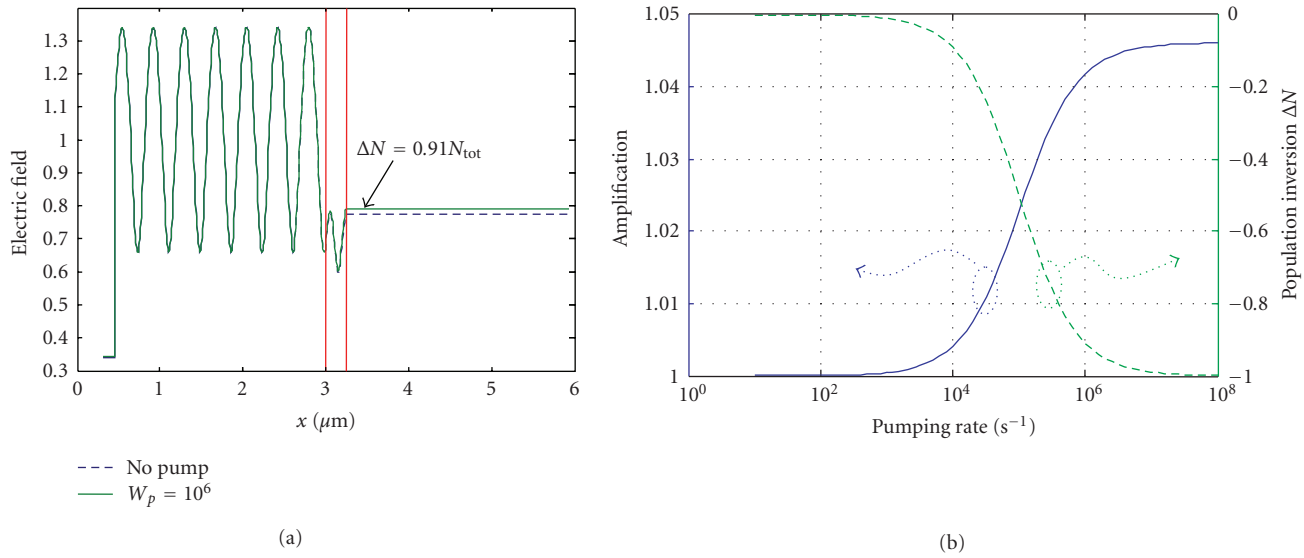

FIGURE 4: (a) Amplitude distributions of electric field across the device, where in the transmitted region, an apparent amplification can be observed under the pump rate of 10^6 compared with no pump case. (b) Amplification of transmitted signal and population inversion ΔN inside the active medium verse the pump rate varying from 10^2 to 10^8.

To study the PL and lasing dynamics in the active system, we introduce randomly distributed sources within the system to simulate the spontaneous emission. Each source generates waves with a Lorentzian spectrum distribution centered at ω_s and amplitude dependent on the population density of N_2. Since spontaneous emission is radiated incoherently, the phase associated with the emission is chosen randomly.

4. NUMERICAL SIMULATIONS OF ACTIVE NANOCRYSTAL DEVICES

The demonstration of photoluminescence in Si-ncs under room temperature is a significant step towards the development of Si-based light emitting materials. The indirect nature of the energy band gap is partially resolved due to quantum confinement in lower-dimension silicon such as Si/SiO_2 superlattices, porous silicon, Si-ncs embedded in SiO_2, and rare earth-doped Si-ncs.

Based on the extensive experimental measurements of Si-ncs, the principle structural, and optical parameters, such as emission life time, absorption cross-section, emission cross-section, emission linewidth, and peak wavelength can be deduced, as listed in the following table [10, 21].

TABLE 1: Optical properties and simulation parameters of Si-ncs.

Pump wavelength (nm)	532
Pump photon flux $I_p/\hbar\omega$ ($cm^{-2}\,s^{-1}$)	$10^{15}\sim10^{22}$
Absorption cross-section σ_p (cm^2)	10^{-14}
Emission cross-section σ_s (cm^2)	3×10^{-16}
Si-nc concentration N_{tot} (m^{-3})	6×10^{24}
Emission wavelength λ (nm)	750
Emission spectrum linewidth (nm)	200
τ_{10} (s)	10^{-15}
τ_{21} (s)	10^{-5}
τ_{32} (s)	10^{-15}
Refractive index of Si-ncs	$1.9 + i0.0014$
Refractive index of SiO_2	1.454

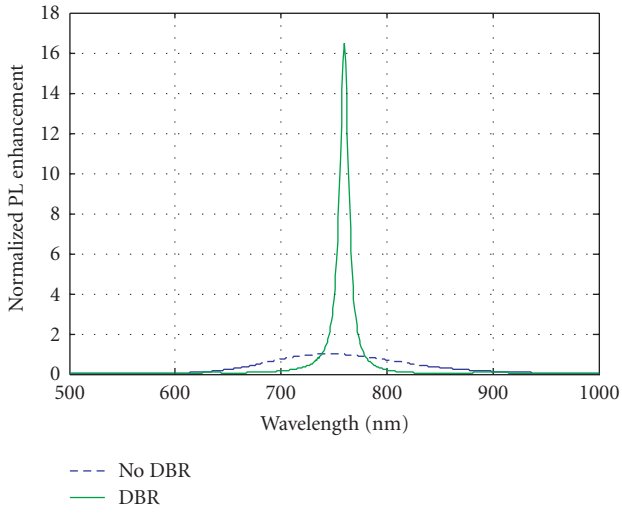

Figure 5: Enhanced amplified spontaneous emission (PL) with microcavity consisting of 1D DBRs with the layers of $N_u = 4$ and $N_d = 6$ compared with the one without DBR.

In simulations, the active medium is uniformly pumped with a shorter wavelength source, that is, 457 nm, and the pump photon flux, $I_p/\hbar\omega$, varies from $10^{15}\sim10^{22}\,\mathrm{cm}^{-2}\mathrm{s}^{-1}$. Then, the pump rate, $W_p = \delta_p I_p/\hbar\omega$, can be determined as $10\sim10^8\,\mathrm{s}^{-1}$. The effective index of silicon nanocrystals is calculated using Bruggman's effective medium approximation. In this section, we investigate the gain characteristics of Si-ncs in both 1D stacks [25] and 2D waveguiding structures [26] by incorporating the optical and structural properties above as simulation parameters in the coupled rate and electromagnetic wave equations.

4.1. Light amplification and amplified spontaneous emission in 1D nanocrystals

Based on the theoretical model developed in the previous section, we first consider light amplification in Si-ncs by applying pump and probe signal transmission simulation. The structure investigated is a supperlattice of Si/SiO_2 on the top of a quartz substrate, as shown in Figure 3(a). The thickness of Si-nc is 250 nm. In the FDTD simulation, the mesh size is 20 nm, and the time step is 2.25×10^{-17} seconds.

First, we consider a continuous plane wave with a wavelength of 750 nm illuminating the sample from free space. The steady-state results with two different pump rates are shown in Figure 4(a). The red lines indicate interfaces between Si-ncs and their claddings. The solid and dash lines represent the field distributions across the devices with and without a pump rate of 10^6. In the transmitted region (SiO_2 substrate), an apparent amplification can be identified. To accurately characterize the light amplification of Si-ncs, we calculate the transmittance based on the Poynting vector. Then, the light amplification factor is defined by normalizing the transmitted powers with pump to without pump. In doing so, the interface coupling loss can be subtracted, and consequently, net gain contributed from stimulated emission can be extracted. We plot both the amplification factor and population inversion in Figure 4(b) for pump rates varying from 10^2 to 10^8. As we see from the figure, both the amplification factor and normalized population inversion density are nonlinearly dependent on the pump rate. While the pump rate increases to 10^8, the inversion population density starts to saturate and leads to a maximum amplification factor of 1.046.

In addition to the modeling of stimulated emission for the probe signal amplification through active Si-ncs, we consider photoluminescence and microcavity-based ASE from an Si-nc device, as shown in Figure 3(b). Instead of using an external plane wave, we introduce an artificial source to simulate the spontaneous emission process in an active medium.

The spontaneous emission occurs when electrons spontaneously drop from an upper (N_2) to a lower-energy level (N_1) while emitting electromagnetic radiation at the transition frequency. While atoms emit this kind of fluorescence or spontaneous emission, each individual atom acts exactly like a small random oscillating radiator. Each atom radiates independently, with a temporal phase angle that is independent of all the other radiating atoms. To model this process, we introduce many dipole sources randomly distributed within the system in the FDTD simulation. Each source generates waves in the form of a Lorentzian spectrum distribution centered at 750 nm, with its amplitude dependent on the time varying population density of N_2. Since the spontaneous emission is incoherent, the phase associated with the photon is random, and thus we code a random phase to each dipole source in the FDTD modeling. To attain the PL characteristics of Si-nc, a few detectors are placed to collect temporal photon luminescence both in free space and the quartz substrate. The recorded temporal electromagnetic waves are Fourier transformed to the frequency domain in order to obtain the PL spectrum.

It is well known that the spontaneous emission is not only determined by the active material, but it also relates to the optical structure. By introducing a microcavity, we can control and manipulate the spontaneous emission. Based on photonic crystal band gap materials, many microcavities have been designed to enhance the spontaneous emission in active material systems [27]. The simplest configuration consists of planar stacks of alternating high- and low-index thin films deposited using conventional planar fabrication processing, such as PECVD [9]. To this end, we designed a Fabry-Perot resonator consisting of one-dimensional photonic crystal structures to confine the optical mode inside the active Si-nc material, as shown in Figure 3(b). The device consists of Si-ncs sandwiched with some variable number of periods of a one-dimensional PhC lattice at both ends, that is, N_u and N_d. To form a band gap within the PL spectrum, Si_3N_4 and SiO_2 are used as alternate high- and low-index materials with their indices of 2.05 and 1.454 at the wavelength of 750 nm. The lattice period is designed as 210 nm and the filling factor of Si_3N_4 is chosen as 50%. Transmission characteristics have been performed to confirm that a band gap opens between 638 and 879 nm. With a 250 nm thick Si-nc medium as a defect, a strong single-cavity

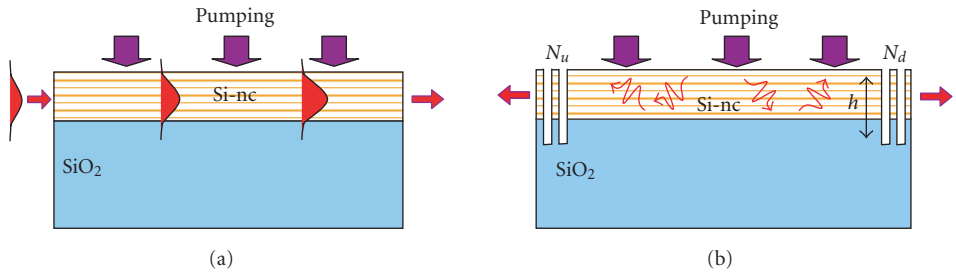

Figure 6: (a) Configuration for waveguide amplification study. A Gaussian pulse in air is incident on a pumped Si-nc waveguide. A detector in air at the end of the waveguide measures the amplification by normalizing to the output without pumping. (b) Configuration for amplified spontaneous emission study. Optional DBRs create a microcavity to enhance spontaneous emission of pumped Si-ncs.

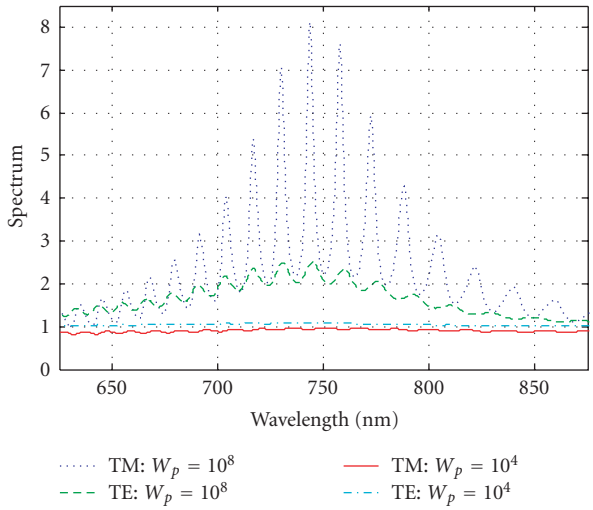

Figure 7: Amplification through a pumped Si-nc waveguide for TE and TM cases. Detected signal under pumping is normalized to detected signal without pumping to eliminate loss due to reflection at waveguide interfaces.

mode located at a wavelength of 751 nm can be recognized within the band gap. The Q factor is measured as 85 while the numbers of DBRs are $N_u = 1$ and $N_d = 6$.

Applying the modeling tools developed in this work, we performed numerical simulations to illustrate the enhancement effect of spontaneous emission due to the introduction of a microcavity in an active Si-nc system. During the time evolution of the population densities, the population inversion is found to be $\Delta N = 5.4 \times 10^{24}$ after the system reaches steady state. A comparison of spontaneous emission spectra with and without DBR measured in the free space is illustrated in Figure 5. All the spectra are normalized to the peak PL intensity of Si-nc devices without DBR. As we can see from the figure, the PL spectrum without DBR shows a typical broad emission band of 250 nm centered at 750 nm. By introducing the microcavity, a sharp emission enhancement can be observed. The resonant wavelength is slightly redshifted to a longer wavelength at 760.1 nm and the linewidth becomes smaller (7.2 nm). The peak PL exhibits an enhancement factor of 16.4.

Owing to the large reflectance of DBR mirrors, the optical field at resonance is well confined inside the microcavity. As a consequence, the resonant optical mode has a longer photon lifetime and thus longer interaction with the gain medium resulting in the enhanced PL signal at the resonant wavelength.

In addition to the study of active characteristics in 1D Si-ncs, we are also interested in edge emission from nanocrystals, in which a two-dimensional (2D) system is required. In the following section, we will investigate Si-nc waveguiding structures for this application.

4.2. Light amplification and amplified spontaneous emission in nanocrystal waveguiding structures

In two dimensions, we consider an active planar waveguide made of higher index Si-nc in a SiO_2 matrix on top of a lower index SiO_2 substrate. Both TE and TM propagations are simulated to identify their amplification and ASE characteristics. In cases where we study spontaneous emission, dipole sources representing the spontaneous emission source have freedom to emit in any direction. Gain guiding and total internal reflection (TIR) combine to direct the spontaneous emission along the length of the Si-nc region.

The basic 2D geometry we consider consists of a slab waveguide composed of a 200 nm Si-nc layer on a SiO_2 substrate surrounded by air. We now consider two devices based on this geometry as shown schematically in Figure 6.

The first device is a waveguide amplifier, shown in Figure 6(a). In this case, a Gaussian pulse introduced in air couples into the waveguide, propagates along the length of the waveguide, interacts with the pumped active material, and arrives at the detector, positioned in air at the opposite end. To study the waveguide's behavior as an amplifier, we normalize the detected signal at various pump strengths to the signal when the pumping and material losses are set to zero. This allows us to study amplification without loss due to reflections at the interfaces. The normalized amplification for a 10 μm waveguide is shown in Figure 7 for the TE and TM cases at two pump rates. Both the TE and TM cases exhibit amplification under sufficient pumping, although the TM case is clearly stronger. This can be understood by considering the TE mode profile which includes a longer evanescent tail, extending into the substrate. The broader

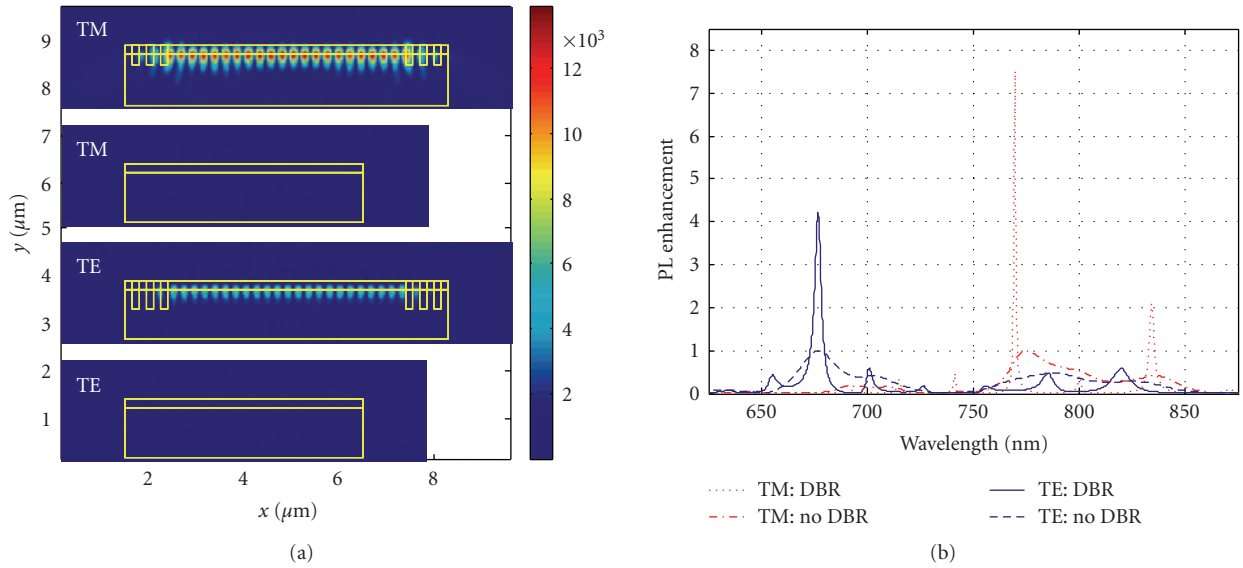

Figure 8: DBRs enhance PL signal of Si-ncs by ~4X in the TE case and ~8X in the TM case. (a) The steady-state amplitude of the E_z component is shown, the TM case corresponds to the peak wavelength of ~770 nm while the TE case corresponds to its peak wavelength of 677 nm. (b) The spectral response for TE and TM with 3 periods of DBRs is shown and normalized to the peak PL emission for the no-DBR case.

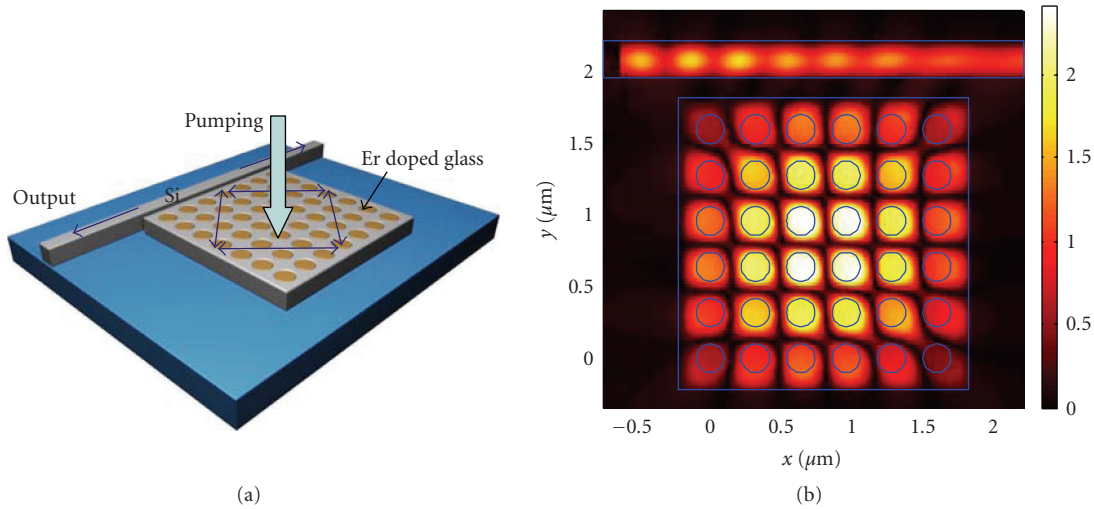

Figure 9: (a) Schematic of silicon laser based on dispersion-engineered photonic crystals where the active material is introduced by backfilling the air holes of the PhC. (b) The highest cavity mode below the band edge.

mode results in a reduced modal volume in the Si-nc region where amplification is possible; consequently amplification of the TE mode is reduced relative to the more confined TM mode. The oscillations in the spectral response of both modes are due to Fabry-Perot effects. The high-index contrast Si-nc to air interface introduces enough reflection to create a weak microcavity.

The second device shown in Figure 6(b) employs two DBRs to enhance the Fabry-Perot microcavity which introduced oscillations in the amplification spectrum studied above. The DBR microcavities are considered for their role in an ASE device. Spontaneous emission is modeled as dipole sources with random phase positioned throughout the Si-nc region. The PL spectrum is detected in air to the right of the waveguide. Each DBR consists of alternating layers of air and Si-nc/SiO_2 with a period of 300 nm, optimized to open a band gap between 650 nm and 900 nm. The air holes are "etched" through the Si-nc region and 200 nm into the SiO_2 region to create the DBR. The detected PL signal with DBR is normalized to the peak PL signal without DBR. A 5 μm Si-nc region is bordered by 3 periods of DBR on either side. The resulting ASE for the TE and TM cases is shown in Figure 8. The steady-state response at the peak wavelength shows the high-optical confinement within the microcavity.

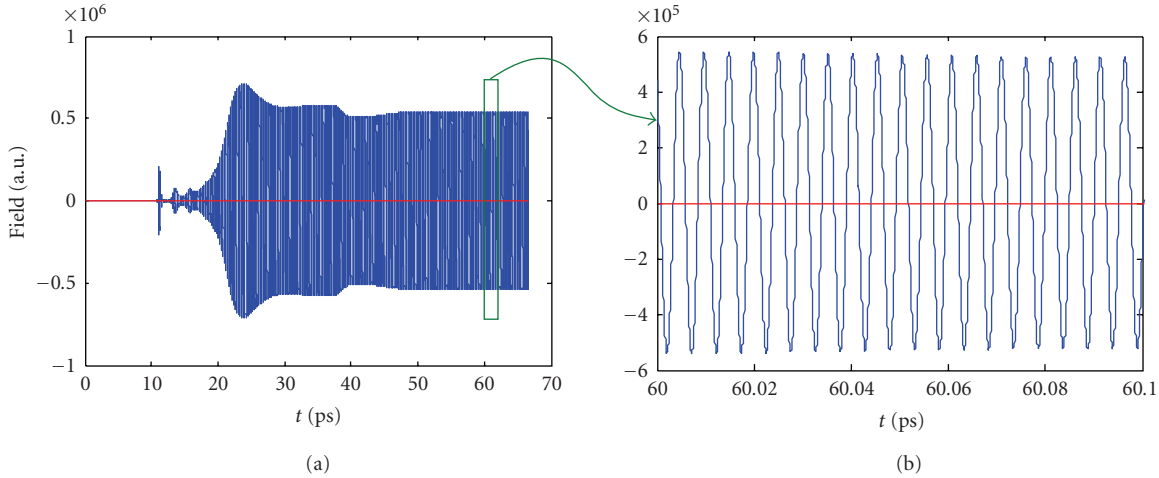

Figure 10: (a) Lasing dynamics by monitoring output in the straight dielectric waveguide, (b) steady-state output of single optical mode as shown within the time window in (a).

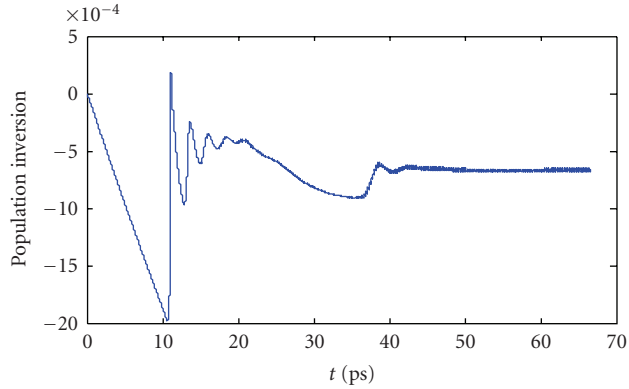

Figure 11: Normalized population inversion at pump rate of 2×10^8/s.

The inclusion of DBRs enhances the PL signal by a factor of 4 in the TE case and nearly a factor of 8 in the TM case.

5. LASING DYNAMICS IN A PHOTONIC CRYSTAL-BASED SILICON MICROCAVITY

In this section, we employ the developed technique to investigate the time evolution of population density functions and electromagnetic dynamics of a novel photonic crystal-based microcavity. During the lasing activity, the strong feedback of the local light intensity saturates the amplification in the system through the nonlinearity of active material, and eventually leads to a steady optical mode output.

Light propagation in a PhC is most appropriately interpreted through a dispersion diagram, which characterizes the relationship between the frequency of the wave, ω, and its associated wave vector, k. Dispersion surfaces provide the spatial variation of the spectral properties of a certain band within the photonic crystal structure. An electromagnetic wave propagates along the direction normal to the dispersion surface, which stems from the relation of the group velocity $\mathbf{v}_g = \nabla_k \omega(\mathbf{k})$. The ability to shape the equifrequency contours (EFC), and thereby engineer the dispersion properties of the PhC, opens up a new paradigm for the design of optical devices [28–30]. For the applications of self-collimation, we desire a flat EFC, in which case the wave is only allowed to propagate along those directions normal to the sides of the straight curvatures. As such, it is possible to vary the incident wave vector over a wide range of angles and yet maintain a narrow range of propagating angles within the PhC.

Based on the dispersion waveguiding property in photonic crystals, a novel class of photonic-crystal-embedded microcavity (PCEM) coupled with waveguide [30] has been theoretically investigated using FDTD algorithm, in which both optical resonant mode and quality factor are particularly considered. Figure 9(a) depicts the schematic of our design. A photonic crystal cavity consists of a silicon square slab perforated by an $N \times N$ array of square lattice. The air holes are back-filled with the gain medium, that is, Er-doped glasses, as shown in the inset of Figure 9(a). The hole has a radius of $0.3a$, where a is the lattice constant. The silicon and glass have refractive indices of 3.5 and 1.5, respectively. After the light couples into the resonator from the waveguide, it will propagate along the ΓM direction and then will be reflected at the edge of the resonator. As such, with the assistance of the four clear edges of silicon slab as mirrors, a traveling wave-based cavity can be formed along the optical path indicated by an arrow loop in Figure 9(b), which is similar to a whispering gallery mode in a microdisk resonator. Along one edge of this microcavity, a conventional dielectric waveguide is used for the in-/outcoupling between the cavity and waveguide. To realize the active operation in such a microcavity, we fill the air holes with a certain gain medium to achieve nonlinear gain dynamics. In our design, low-index highly doped Erbium Ion glass is considered as a gain material for the light amplification. The proposed device has several advantages. (1) Since we are working at the first band of the dispersion surface, the self-collimation

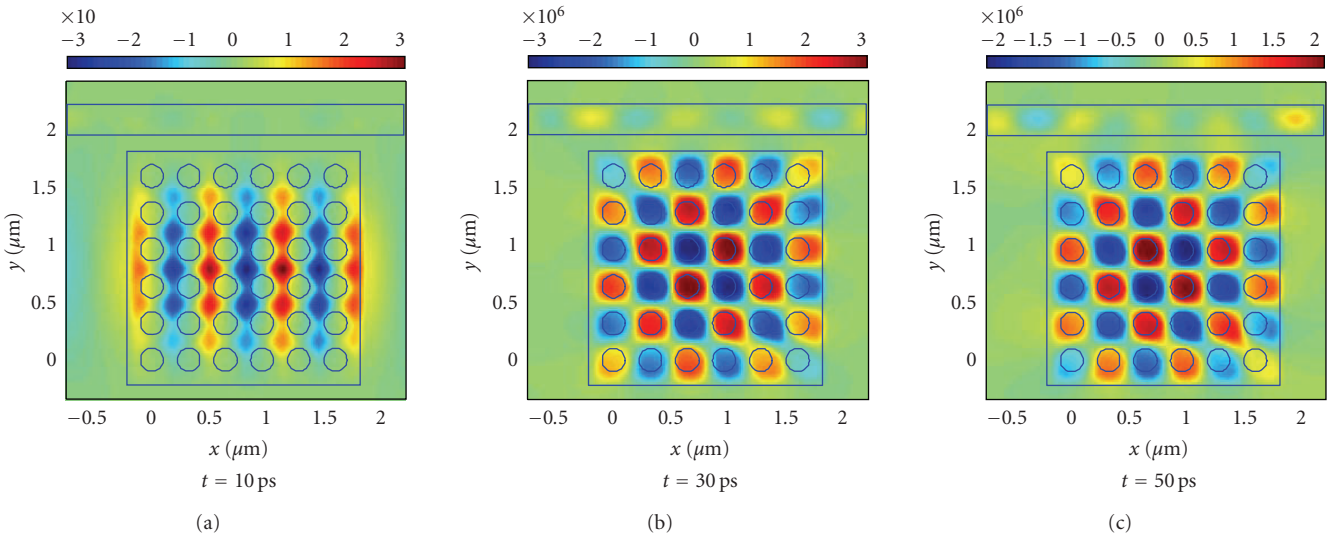

Figure 12: Snapshots of 2D field distribution at three time instants: 10, 30, and 50 ps.

mode is far below the light cone, therefore the wave inside the resonator is well confined inside the slab with minimal out-plane propagation loss even with the presence of a substrate. (2) The self-collimation mode is very close to the band edge, so the slow group velocity will enhance the nonlinear interaction between light and gain material.

We simulate the proposed device using the FDTD method. A 6×6 array of glass-filled cylinders is initially simulated; the highest resonant mode below the band edge of the first dispersion band is shown in Figure 9(b). We observe that most optical modes are well confined within the low-index materials. This unique property may benefit the lasing mechanism and lower the optical pumping threshold. The cavity properties are largely dependent on the design parameters, such as gap size between the waveguide and resonator, and array size. An extensive study has been performed to investigate the passive cavity performance. The gap between the cavity and waveguide is a critical design parameter to achieve optimal coupling and Q factor. An optimal gap size of 160 nm is found in the following design. In this case, we measured a Q factor of 520 and drop efficiency of 32.2% for a resonant mode at 1532 nm. We also investigate the Purcell factor as an additional figure of merit for the microcavity. The Purcell factor dictates the enhancement in the radiative recombination rate due to optical confinement provided by the cavity. Based on the mode profile at the resonant wavelength of 1532 nm, the PhC microcavity exhibits an effective mode volume of $3.27^*(\lambda/n)^3$ and a Purcell factor of 10.88.

With the appropriate design of the microcavity based on the dispersion engineering of photonic crystals, we further considered backfilling the air holes in photonic crystals with a gain medium, that is, Er-doped glass, to achieve active operation, as shown in the schematic view of the proposed novel silicon laser in Figure 9(a). For the Er^{3+} Ion, the typical lifetime is on the order of $10^{-3} \sim 10^{-2}$ s. Numerically, using a rigorous EM algorithm in the time domain to simulate the lasing dynamics, this is far beyond the state-of-the-art computational capability, particularly in a high-dimension system. To phenomenologically investigate the lasing dynamics in the microcavity with the backfilled gain medium, we scale the lifetime of electron population transition accordingly while maintaining a reasonable timescale associated with different relaxation processes. To this end, we shorten the lifetime of atomic transitions to reduce the computation time necessary to achieve the steady state. The lifetimes are given by $\tau_{10} = 10^{-12}$ s, $\tau_{21} = 10^{-10}$ s, and $\tau_{32} = 10^{-13}$ s. The transition frequency associated with the energy levels N_2 and N_1 is chosen as 200 THz and linewidth is taken to be 6 THz. The pump rate into level N_3 is chosen as $W_p = 2 \times 10^8$/s. The initial state of the simulation is included as follows: all the electrons are in the ground state, so there is no field in the cavity and no spontaneous emission. In this paper, we choose $N_0 = 3 \times 10^{24}/\text{m}^3$. After the electrons are pumped, the system starts to evolve both in terms of population densities and electromagnetic waves. To monitor the EM dynamics, a detector is placed in the waveguide.

In the FDTD simulation, a total time of 66 ps is simulated. The time step Δt is chosen as 3.3×10^{-7} s, so a total of 2 million FDTD iterations are used. The evolution of electromagnetic waves starts from an initial small noise current over the photonic crystal cavity. A detector is placed in the waveguide to monitor the lasing dynamics, and the total field in the output waveguide is illustrated in Figure 10(a). In the figure, we observe the lasing performance. For clarity, we zoom in on a portion of the transient plot near 60 ps as shown in Figure 10(b), which indicates a nearly single lasing mode.

Figure 11 shows the calculated time evolution of the electron population inversion between energy levels 2 and 1 at the position of one of the central holes in the cavity. The plotted population inversion is normalized to total electron concentration. During the simulation, the ground state population density remains relatively unchanged compared

to higher-level populations. In the beginning, the population inversion linearly increases, leading to significant amplification of electromagnetic waves in the cavity. In the meantime, the desired cavity mode is gradually established. Eventually, a convergent population inversion, -6.9×10^{-4}, can be observed. The population dynamics are consistent with the lasing output from the waveguide.

In addition, snapshots of the 2D magnetic fields after the simulation ran for 10, 30, and 50 ps are plotted in Figure 12, where the lasing dynamics of the electromagnetic field is gradually established within the cavity. In the end, the high-intensity distribution of EM field can be observed in the cavity area, particularly in the low-index material region and steady results are output from both ends of the straight waveguide.

6. CONCLUSION

In this paper, a time-domain analysis of active silicon-based photonic devices is proposed. The simulation model couples Maxwell's equations with the rate equations to fully describe the nonlinearity of active medium, and numerically solves them using an ADE-FDTD scheme. Both stimulated and spontaneous emissions are taken into account in the active medium system. Light amplification characteristics due to stimulated emission are investigated under various pump rates in both 1D and 2D waveguiding silicon nanocrystals. To achieve amplified spontaneous emission, microcavities based on photonic band gap materials are carefully designed. These Fabry-Perot microcavities are shown to significantly enhance the spontaneous emission signal. At last, we propose a novel PhC-based microcavity, in which a low-index gain medium is incorporated into the air holes in photonic crystals, to study the lasing characteristics.

ACKNOWLEDGMENT

This work is partially sponsored by the research Contracts FA9550-06-1-0470 and 5710002024 from AFOSR.

REFERENCES

[1] B. Jalali, M. Paniccia, and G. Reed, "Silicon photonics," *IEEE Microwave Magazine*, vol. 7, no. 3, pp. 58–68, 2006.

[2] L. Pavesi, "Will silicon be the photonic material of the third millenium?" *Journal of Physics: Condensed Matter*, vol. 15, no. 26, pp. R1169–R1196, 2003.

[3] M. E. Castagna, S. Coffa, M. Monaco, et al., "Si-based materials and devices for light emission in silicon," *Physica E*, vol. 16, no. 3-4, pp. 547–553, 2003.

[4] L. Pavesi, L. Dal Negro, C. Mazzoleni, G. Franzò, and F. Priolo, "Optical gain in silicon nanocrystals," *Nature*, vol. 408, no. 6811, pp. 440–444, 2000.

[5] A. Fojtik, J. Valenta, I. Pelant, M. Kalal, and P. Fiala, "On the road to silicon-nanoparticle laser," *Journal of Materials Processing Technology*, vol. 181, no. 1–3, pp. 88–92, 2007.

[6] D. J. Lockwood, Z. H. Lu, and J.-M. Baribeau, "Quantum confined luminescence in Si/SiO_2 superlattices," *Physical Review Letters*, vol. 76, no. 3, pp. 539–541, 1996.

[7] V. Ovchinnikov, A. Malinin, V. Sokolov, O. Kilpelä, and J. Sinkkonen, "Photo and electroluminescence from PECVD grown a-Si:H/SiO_2 multilayers," *Optical Materials*, vol. 17, no. 1-2, pp. 103–106, 2001.

[8] J. Lee, J. H. Shin, and N. Park, "Optical gain at 1.5 μm in nanocrystal Si-sensitized Er-doped silica waveguide using top-pumping 470 nm LEDs," *Journal of Lightwave Technology*, vol. 23, no. 1, pp. 19–25, 2005.

[9] T. Creazzo, E. Marchena, B. Redding, T. Hodson, and D. W. Prather, "Fabrication and characterization of silicon/silicon dioxide super lattices for silicon based light emitting devices," in *Nanoengineering: Fabrication, Properties, Optics, and Devices IV*, vol. 6645 of *Proceedings of SPIE*, pp. 1–8, San Diego, Calif, USA, August 2007.

[10] L. Pavesi, S. Gaponenko, and L. Dal Negro, *Towards the First Silicon Laser*, Kluwer Academic Publishers, Dordrecht, The Netherlands, 2002.

[11] H. Rong, R. Jones, A. Liu, et al., "A continuous-wave Raman silicon laser," *Nature*, vol. 433, no. 7027, pp. 725–728, 2005.

[12] O. Boyraz and B. Jalali, "Demonstration of a silicon Raman laser," *Optics Express*, vol. 12, no. 21, pp. 5269–5273, 2004.

[13] A. S. Nagra and R. A. York, "FDTD analysis of wave propagation in nonlinear absorbing and gain media," *IEEE Transactions on Antennas and Propagation*, vol. 46, no. 3, pp. 334–340, 1998.

[14] X. Jiang and C. M. Soukoulis, "Time dependent theory for random lasers," *Physical Review Letters*, vol. 85, no. 1, pp. 70–73, 2000.

[15] P. Sebbah and C. Vanneste, "Random laser in the localized regime," *Physical Review B*, vol. 66, no. 14, Article ID 144202, 10 pages, 2002.

[16] S. Shi and D. W. Prather, "Lasing dynamics of a silicon photonic crystal microcavity," *Optics Express*, vol. 15, no. 16, pp. 10294–10302, 2007.

[17] S. Shi, G. Jin, and D. W. Prather, "Electromagnetic simulation of quantum well structures," *Optics Express*, vol. 14, no. 6, pp. 2459–2472, 2006.

[18] D. Biallo, A. D'Orazio, M. De Sario, V. Petruzzelli, and F. Prudenzano, "Time domain analysis of optical amplification in Er^{3+} doped SiO_2-TiO_2 planar waveguide," *Optics Express*, vol. 13, no. 12, pp. 4683–4692, 2005.

[19] S.-H. Chang and A. Taflove, "Finite-difference time-domain model of lasing action in a four-level two-electron atomic system," *Optics Express*, vol. 12, no. 16, pp. 3827–3833, 2004.

[20] K. K. Lee, D. R. Lim, H.-C. Luan, A. Agarwal, J. Foresi, and L. C. Kimerling, "Effect of size and roughness on light transmission in a Si/SiO_2 waveguide: experiments and model," *Applied Physics Letters*, vol. 77, no. 11, pp. 1617–1619, 2000.

[21] L. Dal Negro, M. Cazzanelli, N. Daldosso, et al., "Stimulated emission in plasma-enhanced chemical vapour deposited silicon nanocrystals," *Physica E*, vol. 16, no. 3-4, pp. 297–308, 2003.

[22] A. E. Siegman, *Lasers*, University Science Books, Mill Valley, Calif, USA, 1986.

[23] J.-Y. Sung, A. Tewary, M. L. Brongersma, and J. H. Shin, "Cavity Q measurements of silica microspheres with nanocluster silicon active layer," *IEEE Journal on Selected Topics in Quantum Electronics*, vol. 12, no. 6, pp. 1388–1392, 2006.

[24] L. Dal Negro, M. Cazzanelli, B. Danese, et al., "Light amplification in silicon nanocrystals by pump and probe transmission measurements," *Journal of Applied Physics*, vol. 96, no. 10, pp. 5747–5755, 2004.

[25] S. Shi, T. Creazzo, B. Redding, and D. W. Prather, "Simulation of light amplification and enhanced spontaneous emission in silicon nanocrystals," in review, *Journal of Optics A: Pure and Applied Optics*, 2008.

[26] B. Redding, S. Shi, and D. W. Prather, "Time analysis of active silicon nanocrystal waveguiding structures," *Optics Express,* accepted for publication, 2008.
[27] A. Belarouci and F. Gourbilleau, "Microcavity enhanced spontaneous emission from silicon nanocrystals," *Journal of Applied Physics*, vol. 101, no. 7, Article ID 073108, 4 pages, 2007.
[28] D. W. Prather, S. Shi, D. M. Pustai, et al., "Dispersion-based optical routing in photonic crystals," *Optics Letters*, vol. 29, no. 1, pp. 50–52, 2004.
[29] M. R. Newton, K. A. Morey, Y. Zhang, et al., "Anisotropic diffusion in face-centered cubic opals," *Nano Letters*, vol. 4, no. 5, pp. 875–880, 2004.
[30] K. Tsia and A. Poon, "Dispersion-guided resonances in two-dimensional photonic-crystal-embedded microcavities," *Optics Express*, vol. 12, no. 23, pp. 5711–5722, 2004.